Laser Frequency Stabilization using a Microcontroller

by

Kamal A. Shalaby

A THESIS SUBMITTED IN PARTIAL FULFILLMENT OF THE REQUIREMENTS FOR THE DEGREE OF

Bachelor of Science

Supervisor(s):	Dr. Brynle Barrett, Assistant Professor, Dept. of Physics
Examining Board:	Dr. P. T. Jayachandran, Professor, Dept. of Physics, Chair
	Dr. Ben Newling, Professor, Dept. of Physics
	Dr. Igor Mastikhin, Professor, Dept. of Physics
	Dr. Zong Chao Yan, Professor, Dept. of Physics

THE UNIVERSITY OF NEW BRUNSWICK

March, 2022

Acknowledgements

I would like to express my gratitude for my supervisor, Dr. Brynle Barrett, for his guidance and leadership throughout my honours project.

Table of Contents

List of Tables

List of Figures

Chapter 1

Introduction

Lasers are ubiquitous in modern technology, from laser printers and barcode scanners, to land survey equipment and optical communication systems. Lasers are also used extensively in scientific research across several domains, including physics, biology, chemistry, mechanical engineering, and space science. Each research area has its own specific requirements for a laser's operating parameters, such as the wavelength, linewidth, tunable frequency range, available optical power, and polarization purity. Atomic, molecular, and optical (AMO) physics experiments [15, 16], and quantum instruments that rely on the interaction between light and matter [12, 14], often have the most stringent requirements on these parameters.

As an example, consider the requirements for atomic fountain clocks based on laser-cooled cesium atoms. These quantum clocks which currently serve as the primary standard for the definition of the SI second [13] require continuous-wave lasers operating at precisely 852.347275 nm, with a linewidth < 1 MHz, frequency tuning range > 500 MHz, optical power of approximately 200 mW, and a polarization purity > 25 dB (where 0 dB represents completely random polarization). These challenging conditions must also remain "stable" over extended measurement periods of weeks to months, which is a crucial factor when contributing to international timebase and

frequency standards.

Most AMO physics experiments involve the excitation of atoms with light in some way. Many chemical species have optical transitions in the visible to near infrared range of 500–900 nm and since the invention of the laser in 1960, a variety of coherent light sources have been developed that cover this range. However, in the mid-1990s semiconductor diode lasers [18] began gaining popularity and have now been adopted by most atomic physicists. Due to their low cost, simplicity, wavelength coverage, and relatively good performance characteristics (i.e., optical powers of tens of milli-watts and linewidths around 1 MHz), they have become the ideal choice for addressing resonances in many species of atoms and molecules. However, the key aspect in most of these experiments is the ability to precisely tune and stabilize the laser's operating frequency.

The degree to which the laser's frequency must be stabilized depends on the application. For instance, the near-infrared transitions in hot gases can be broadened to > 1 GHz by the thermal distribution of velocities. A laser stabilized at the 1 GHz level is often sufficient to perform many types of experiments. However, the width of the transitions in ultra-cold gases is given by the natural linewidth (typically 5-10 MHz for alkali metals). Thus, for the laser-cooled cesium clock mentioned above, the laser must be stabilized to a much lower level than in a hot gas.

In this thesis, we describe an approach to stabilize a commercial diode laser operating at 780 nm to a hyperfine transition in a room temperature rubidium (Rb) gas. Using Doppler-free absorption spectroscopy, we observe narrow spectral lines that serve as optical references to lock the laser. By modulating the frequency of the laser and feeding the resulting absorption signal into a lock-in amplifier, we generate an error signal with a zero-crossing at the peak of the spectral line. Inspired by similar work [17], this error signal is sent to a microcontroller that runs a digital proportional-integrator (PI) control algorithm and generates a feedback signal for the laser. A

digital PI controller offers a compact format and flexibility in changing parameters and implementing sophisticated algorithms, compared to their counterparts in analog controllers. We discuss how we characterize this closed-loop feedback system in terms of both short-term and long-term relative frequency stability, and we report its performance. This work is a crucial first step toward the realization of a laser-cooled source of ^{87}Rb atoms in the recently constructed laboratory for Quantum Sensing and Ultracold Matter (QSUM) at UNB.

The remainder of this thesis is organized as follows. In Chapter 2, we present what is Doppler free spectroscopy and how to use it to obtain reference optical frequency for our locking system. In Chapter 3, we describe the set up involved and how it is used to lock the laser used to the reference optical frequency. In Chapter 4, we analyze how our lock reacts to different parameters, what are the optimal parameters to ensure the fastest and the most stable locking and the short-term and the long-term stability of the relative frequency. Finally, we provide our conclusions and prospects for future work in Chapter 5.

Chapter 2

Absorption Spectroscopy in Rubidium

2.1 Principles of Atomic Spectroscopy

Atoms consist of a positively-charged nucleus of protons and neutrons surrounded by negatively-charged electrons that are electromagnetically bound to the nucleus. Due to the quantum mechanical properties of electrons, only specific energies are allowed for these bound electron orbits. This gives rise to discrete energy levels known as electronic states. The energy spacing between these states is defined by the specific makeup of the atom (i.e. the number of protons, neutrons and electrons), and is not "easily" changed. Hence, atomic states act as unique quantum signatures specific to a given species. This fact enables astronomers to identify the chemical makeup of distant planets and stars simply by measuring their atomic spectra. Similarly, atomic energy levels can act as absolute references for microwave oscillators, atomic clocks, and other instruments.

Electrons in an atom at rest will tend toward the lowest energy configuration, which is known as the ground state. Electrons can transit between the ground state

and a higher energy "excited state" by absorbing energy equal to the spacing between those states, ΔE. This energy corresponds to one quantum of electromagnetic radiation (known as a photon) at specific frequency ν that is proportional to ΔE through Planck's constant h:

$$\Delta E = h\nu = hc/\lambda.$$

Here, λ is the wavelength of the photon, and c is the speed of light. For most atoms, the energy spacing between the ground state and first excited state corresponds to a frequency of hundreds of terahertz ($\nu \simeq 5 \times 10^{14}$ Hz), hence it is often more convenient to discuss in terms of an optical wavelength ($\lambda = c/\nu \simeq 600nm$).

Electrons can go to a higher energy state by absorbing a photon or go to a lower energy state by emitting a photon in a random direction (a process known as spontaneous emission). The electron transitions can be observed by shining a white light source with a continuous range of frequencies on an atomic gas, as shown in Fig.(2.1) . Some frequencies will be absorbed by the gas. These correspond to the "resonant frequencies" of the atom, and will appear both as dark lines in the transmitted light spectrum and bright lines in the emitted spectrum.

An alternate method to observe atomic resonances is to pass a laser beam with a single optical frequency through the atomic gas. As the laser's frequency is scanned in time, absorption dips or emission peaks can be measured. One can then make a direct correspondence between the known laser frequency and these spectral features to precisely determine the resonance frequency of the atom. For a laser beam propagating through an atomic gas, it will address different classes of atomic velocities. When the laser frequency is below resonance, all the atoms going against the laser beam will see the beam blue-shifted due to the Doppler effect. Some atoms will see the blue-shifted beam in the proper resonance to make the transition. The same is valid for when the scan is above resonance. Atoms going in the same di-

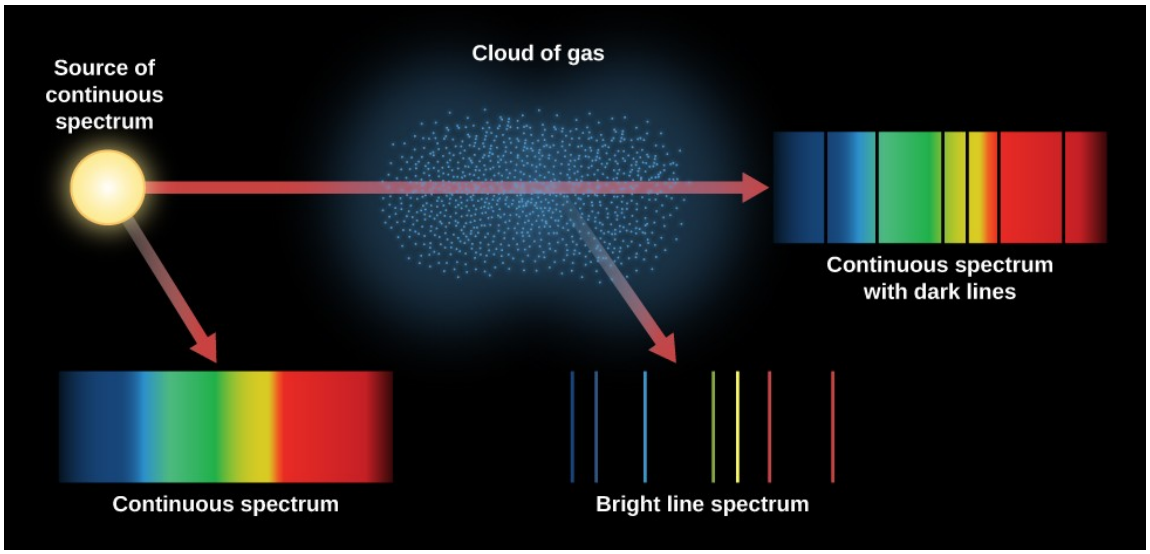

Figure 2.1: Emission and absorption lines of a hypothetical atomic gas. Taken from Ref. [11]

rection as the laser will see it red-shifted, giving some of them the right energy to transition. So scanning the laser frequency around resonance can address a range of velocity classes. A gas of atoms at equilibrium with their surroundings will exhibit a Maxwell-Boltzmann distribution of velocities. This Gaussian distribution has a $1/e$ velocity spread of:

$$\sigma_v = \sqrt{2k_B T/M},$$

where $k_B = 1.38 \times 10^{-23}$ J/K is the Boltzmann constant, T is the temperature of the gas, and M is the mass of the atom. Depending on the atomic gas's temperature, (higher temperatures widen the range of velocities present in the sample), the absorption signal corresponding a single electronic transition will take the form of a Gaussian lineshape centred at the resonance. This effect, where the width of the atomic resonance scales as the square-root of the temperature, is called Doppler broadening of spectral lines. For a gas at room temperature, the Doppler-broadened linewidth is $\Delta_D \simeq \sigma_v/\lambda = 500$ MHz. For many species, this is larger than the spacing between energy levels, making each level impossible to resolve. Cooling the atomic gas to a few kelvins is a potential solution to this problem as it will reduce

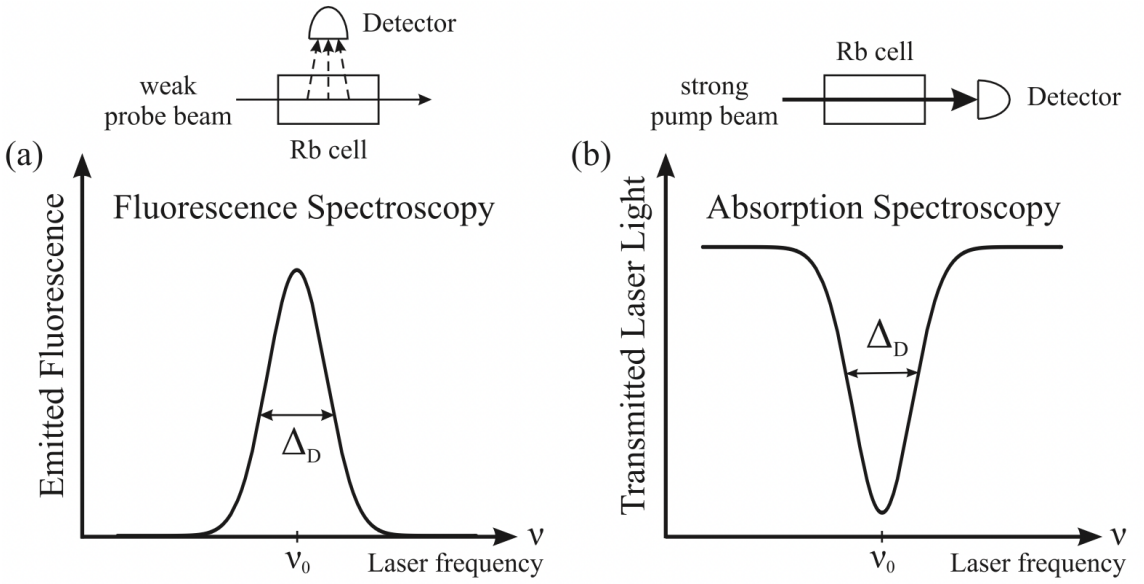

Figure 2.2: Example of a hypothetical (a) emission and (b) absorption spectrum of rubidium atomic vapour. Taken from Ref. [7].

the width of the velocity distribution. However, this method is expensive and is not suitable for most atomic species because they condense into liquid or solid form at such temperatures. There is a simple and effective method to obtain a spectrum that is velocity-independent, and therefore free of Doppler broadening. We discuss this method in the next section.

2.2 Doppler-Free Absorption Spectroscopy

To obtain an absorption signal that is free of Doppler broadening we use two beams with the same frequency, one with a high-intensity (pump beam) while is other is with a low-intensity (probe beam), traveling in opposite directions in the same atomic sample. Figure (2.3) illustrates this scenario for an idealized atom with only one possible electronic transition. The strong pump beam will saturate the transition, maintaining approximately 50% of the atoms on resonance with the pump in the excited state. Let's assume these atoms are at velocity $+v$, as shown in Fig. (2.3)(a)). The weak probe beam, which is at the same frequency as the pump but traveling

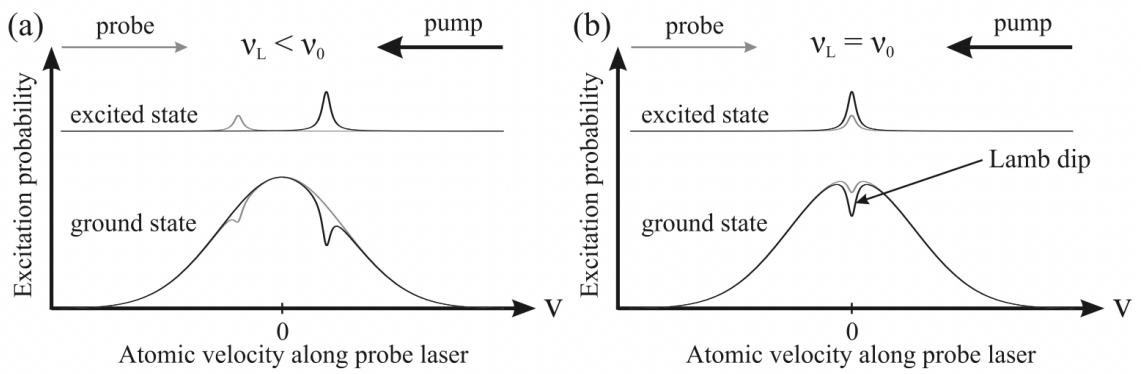

Figure 2.3: Illustration of Doppler-free absorption. A weak probe beam and a counter-propagating strong pump beam excite a gas with a Gaussian distribution of velocities. These idealized atoms have only two levels: a ground and excited state with resonance frequency ν_0. (a) When the laser is below the resonance ($\nu_L < \nu_0$), neither beam excites the same velocity class of atoms. (b) When the laser is on resonance ($\nu_L = \nu_0$), both beams address the zero-velocity class and create a "dip" in the absorption signal. Taken from Ref. [7].

in the opposite direction, will excite atoms with the opposite velocity class as the pump ($-v$). Hence, for non-zero velocities, neither beam addresses the same atoms. So in a graph showing the density of atoms in the excited state against the laser frequency Fig.(2.3), we would find a Maxwell-Boltzmann distribution representing all the different classes of velocity that got excited. The only atomic class both beams will address is the set of atoms that have a zero-velocity component in the direction of the beams. In this case, the zero-velocity atoms excited by pump become partially transparent to the probe—letting more probe light into the detector. This creates a "dip" in the absorption signal when the laser frequency equals the resonance frequency of the atom $\nu_L = \nu_0$. Since each atom's resonance frequency is unique, this simple and reliable method allows us to obtain a narrow spectral line, independent of the temperature of the sample, to which we can "lock" our laser.

2.2.1 Crossover Transitions

Let the laser's frequency be ν, where ν is between two transition frequencies ν_1 and ν_2, where $\nu_1 < \nu < \nu_2$. As the pump beam is propagating through the Rb cell, it

will excite two different velocity classes that sees the ν blue-shifted (if they are going opposite the beam) to ν_2 or red-shifted (if they are going along the beam) to ν_1. The same principle applies for the probe beam. Note that the velocity class that sees the pump beam red-shifted to ν_1 might not be the same velocity class seeing the probe beam blue-shifted to ν_2. An example, if ν were close to ν_1 the velocity component of velocity class does not need to be large in value to see the pump beam red-shifted to ν_1, the same velocity class velocity component will not be enough to see probe beam blue-shifted to ν_2. The only instance both beams will excite the same velocity class if, $\nu = \nu_c$ where,

$$\nu_c = \frac{\nu_1 + \nu_2}{2}. \tag{2.1}$$

Then when $\nu = \nu_c$, the pump beam will excite the atoms to ν_1 and ν_2, while the probe beam goes thorough the excited atoms without being absorbed, showing an extra peak, between the transitions peaks. This peak is called the crossover transition. It only happens when two transitions share the same ground state and are separated by frequencies less than the Doppler width.

2.3 Electronic Structure of ^{85}Rb and ^{87}Rb

We use one of the electronic transitions in rubidium as a reference frequency to lock our laser. Rubidium is chosen for several reasons. First, it has a low melting point of $\sim 40^\circ$ C, and therefore has a sufficient vapour pressure (3×10^{-7} Torr) at room temperature. This feature allows us to do all spectroscopy experiments in a glass cell under standard laboratory conditions. Second, rubidium is an alkali metal, which means it has one valence electron with a simple energy level structure. Third, rubidium has two isotopes, ^{85}Rb (stable) and ^{87}Rb (a lifetime of $\sim 5 \times 10^{10}$ years), with a natural abundance in a 3:1 ratio, where both have similar but distinct energy levels, as shown in Fig.(2.4). These isotopes offer several choices of resonance

frequencies at 780 nm spanning approximately 7 GHz that can serve as potential references for our laser. Finally, and perhaps most importantly, rubidium will be used in future experiments to construct quantum sensors in Dr. Barrett's lab. For that work, it will be crucial to have frequency-stabilized lasers operating close to the various transitions in rubidium. We now describe the basic energy level structure of rubidium shown in Fig.(2.4). For notation purposes, we define n, the principal quantum number, **L**, the electron's orbital angular momentum quantum number, **S**, the electron's spin angular momentum, **J**, a quantum number representing the magnitude of the electron's total angular momentum (**J=L+S**), **I**, the sum of orbital and spin angular momentum of all nucleons, and **F**, the total of all the angular momentum of the atom **F=J+I**.

The valence electron in rubidium lies in a ground state with principal quantum number $n = 5$. The ground state of both isotopes is labelled $5S_{1/2}$, and their first excited states are $5P_{1/2}$ and $5P_{3/2}$, where the labels "S" and "P" correspond to values of the electron's orbital angular momentum ($\mathbf{L} = 0$ and 1, respectively), and the subscripts 1/2 and 3/2 refer to the values of **J**. For this work, we focus on the $5S_{1/2} \rightarrow 5P_{3/2}$ transition in rubidium (known as the D2 line), which occurs at 780.24 nm [4, 5]. This wavelength is within the tuneable range of our diode laser. The D1 line of rubidium ($5S_{1/2} \rightarrow 5P_{1/2}$) occurs much further away at 795 nm.

The splitting of the spectral lines in an atom is called fine structure, and it is due to spin-orbit coupling and the relativistic correction of the Hamiltonian. The positively charged nucleus orbiting the electron (from the reference frame of the electron) creates a current loop that induces a magnetic field. The magnetic field causes torque on the spinning electron to align the electron's magnetic moment with it; this shifts the energy levels, depending on **L** and **S**. For ^{85}Rb and ^{87}Rb, we have $n = 5$ and $\mathbf{L} = 0$ in the ground state. Therefore $\mathbf{J} = 1/2$, hence the ground state for both is called $5S_{1/2}$. For the excited state of both isotopes, $\mathbf{L} = 1$, so **J** ranges

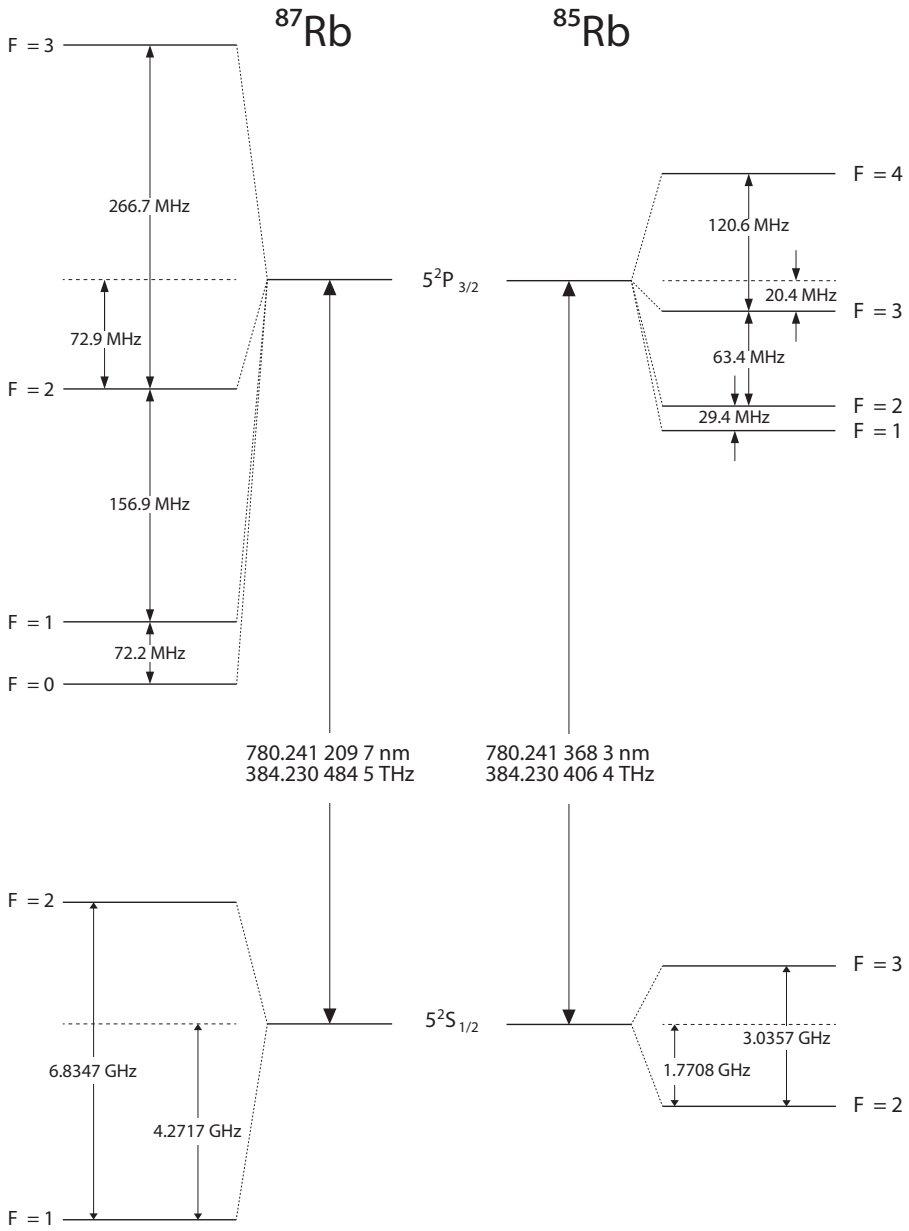

Figure 2.4: The hyperfine structure of ^{85}Rb and ^{87}Rb from $5S_{1/2}$ to $5P_{3/2}$. Taken from Ref. [4, 5]

from $\mathbf{J} = 1/2$ to $\mathbf{J} = 3/2$, giving the two excited states $5P_{1/2}$ and $5P_{3/2}$ (Fig.(2.6)). Diving a step deeper, we find the hyperfine structure. The hyperfine structure is due to the spin-spin coupling between the electron and the nucleus. The spin of the positively-charged nucleus and the negatively-charged electron each create a weak magnetic field that generates a force between these particles. This creates a shift up or down of the energy level, depending on the spin vector orientation of the electron and the nucleus. For ^{85}Rb $\mathbf{I} = 5/2$ and for ^{87}Rb $\mathbf{I} = 3/2$. So, in ^{85}Rb's ground state, $\mathbf{F}$ ranges from $\mathbf{F} = 1$ to $\mathbf{F} = 2$, while ^{87}Rb's $\mathbf{F}$ ranges from $\mathbf{F} = 2$ to $\mathbf{F} = 3$. In the $5P_{3/2}$ excited states of ^{85}Rb, $\mathbf{F} = 1, 2, 3$ and 4 for $5P_{3/2}$. Similarly, in the $5P_{3/2}$ excited state of ^{87}Rb, $\mathbf{F} = 0, 1, 2$ and 3 for $5P_{3/2}$ Fig.(2.4). We will focus primarily on the strongest transitions on the D2 line of rubidium, that is the $\mathbf{F} = 3 \rightarrow \mathbf{F}' = 4$ transition in ^{85}Rb and $\mathbf{F} = 2 \rightarrow \mathbf{F}' = 3$ transition in ^{87}Rb.

2.4 Spectroscopy Measurements in Rubidium

To get the Doppler-free spectrum of Rubidium, two beams of the same frequency go against each other in a Rubidium vapour cell. The main laser beam gets split into two using a glass plate to get two weak beams of the same intensity. Passing the laser beam through a glass plate gets 4% of the laser reflected from each surface, while the rest passes through the plate. The beam that transmits through the plate (i.e., the pump beam, Fig.(2.5) beam 2) is reflected by two mirrors Fig.(2.5), then gets reflected by a polarizing beam splitter (PBS) and passes through the vapour cell. One of the beams reflected off the glass plate (i.e., the probe beam, Fig.(2.5) beam 1), is aligned along the pump beam through the vapour cell. A half-wave plate is placed between the cell and the PBS, which allows us to change the polarization of the probe beam such that it transmits through the PBS onto the photodiode. The probe beam shows the Doppler-broadened transitions including Doppler-free peaks within

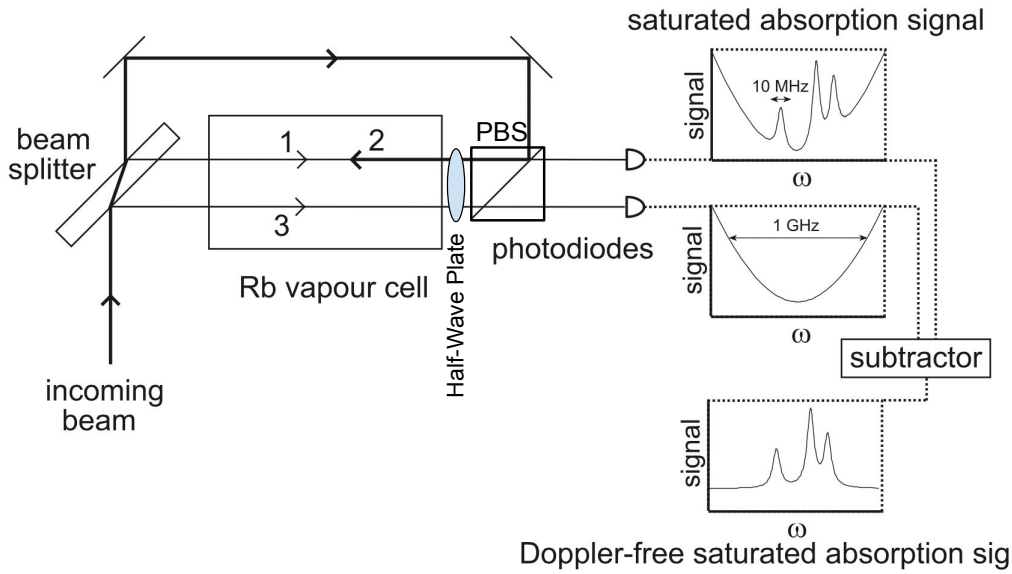

Figure 2.5: The optical setup of Doppler-free saturated absorption spectroscopy. The narrow peaks correspond to Doppler-free hyperfine transitions. Note: the second photodiode is not used in this experiment, however the subtraction procedure will be done in the future experiments to reduce the sensitivity of the lock to laser power fluctuations. Taken from Ref. [6]

the Gaussian background. The beam that reflects off the plate (i.e., the reference beam, beam Fig.(2.5) beam 3), passes through the cell, half-wave plate, and the PBS and falls on another photodiode, containing only the Doppler-broadened peaks. The difference between the photodiodes signals gives the hyperfine structure without the Gaussian-shaped Doppler background.

Figure (2.6) shows the D2 absorption spectrum, this is achieved by scanning the laser's frequency over a range of ~ 8 GHz around ^{85}Rb and ^{87}Rb transitions from $5S_{1/2}$ to $5P_{3/2}$ and capturing the data of the probe beam. Each Doppler-broadened peak in Fig.(2.6(a)) represents a set of hyperfine transitions in one of the isotopes. The small dips in the Doppler peaks show individual hyperfine resonances for the zero-velocity class. By decreasing the range of the laser's scan we zoom in on the ^{85}Rb $F = 3 \rightarrow F' = 1, 2, 3$, where we show most of the hyperfine transitions (except to the $F' = 2$ transition) in the last graph. The sub-Doppler peaks in these data are

fitted as Lorenztian functions, with a Gaussian background, to find the conversion between the scan's time scale and the laser's frequency. Using $F' = 4$ and the crossover (2,4), we found that 9.2 MHz corresponds to 10 ms. With this ratio, the measured linewidth of the $F = 3 \rightarrow F' = 4$ transition was found to be ~ 12 MHz, which is approximately twice the natural linewidth in rubidium ($\Gamma_{\mathrm{N}} = 6$ MHz). This widening in the linewidth is likely due to the intensity of the laser which forces more atoms to the excitation state, broadening the linewidth of a transition, this effect is called Power Broadening[8].

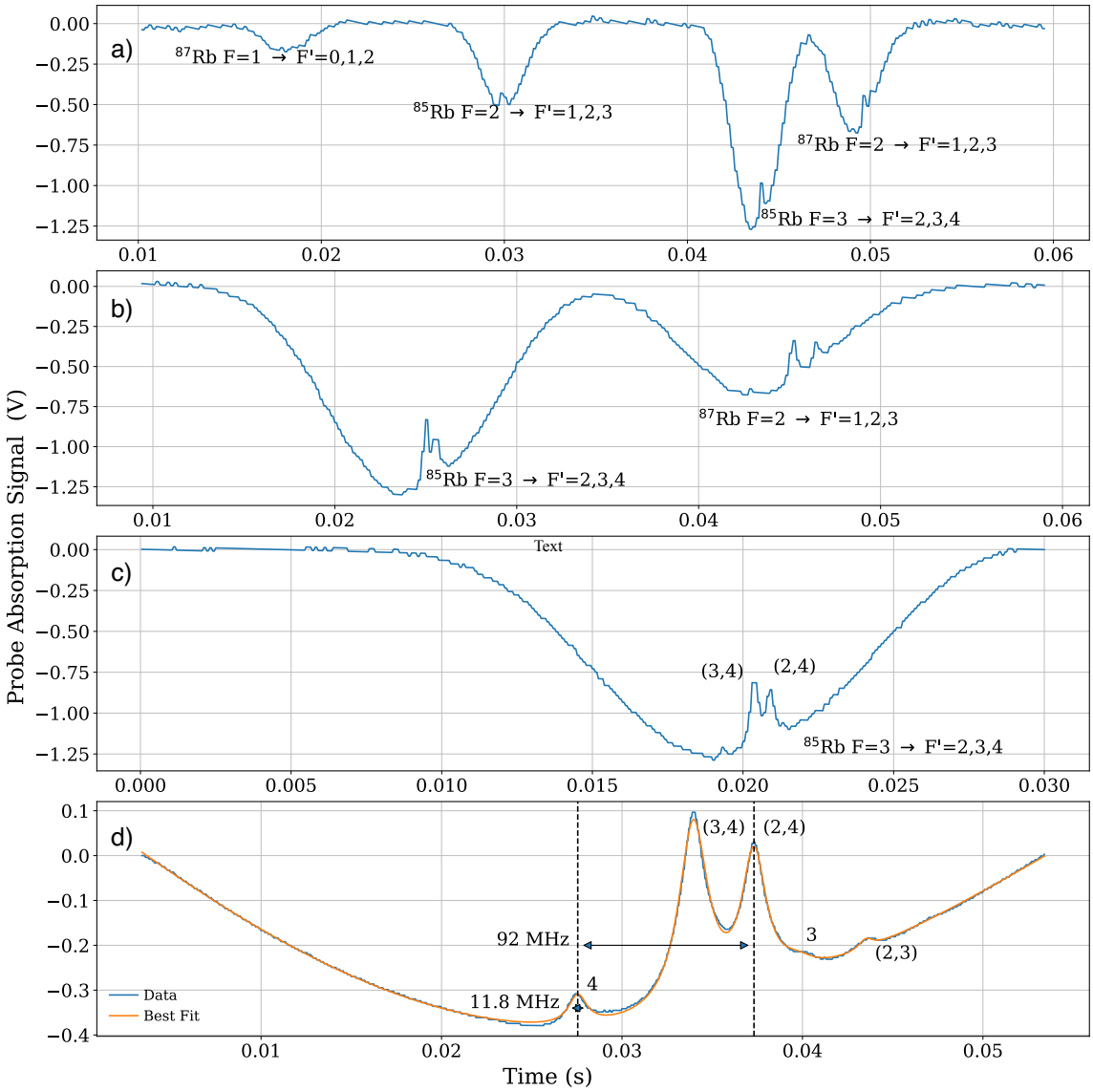

Figure 2.6: (a) ^{85}Rb and ^{87}Rb transitions from $5S_{1/2}$ to $5P_{3/2}$. (b)-(d) Zooming in on the hyperfine structure of ^{85}Rb $F = 3 \rightarrow F' = 2, 3, 4$. (c) The labels next to each peak are the values of F where (3,4), (2,4) and (2,3) are crossover peaks. The 92 MHz represents the frequency separation between the transition to $F = 4$ and the crossover (2,4).

Chapter 3

Laser Frequency Stabilization

3.1 Background

All lasers are susceptible to environmental factors that affect their operating frequency. This is dominated by length contraction/expansion of the laser cavity due to ambient temperature variations. To operate at a single optical frequency, the temperature of the cavity must be actively stabilized.

Modern semiconductor diode lasers come in a compact form factor (e.g. the butterfly mount, Fig.(3.1). Due to their small size and low thermal inertia, they are even more susceptible to temperature variations than their larger counterparts. Similar to light-emitting diodes, these lasers operate by passing a current across the diode's P-N junction, where electrons combine with holes and emit light over a narrow range of wavelengths [1]. Both the optical frequency and power are determined by this "pump" current, hence a stable and low noise current source is paramount to achieving a "narrow linewidth" single-frequency laser.

Our laser (a distributed feedback diode laser operating at 780 nm) is mounted on a commercial circuit board integrated with low-noise current and temperature controllers. This "laser controller" allows simple control of the current and temperature

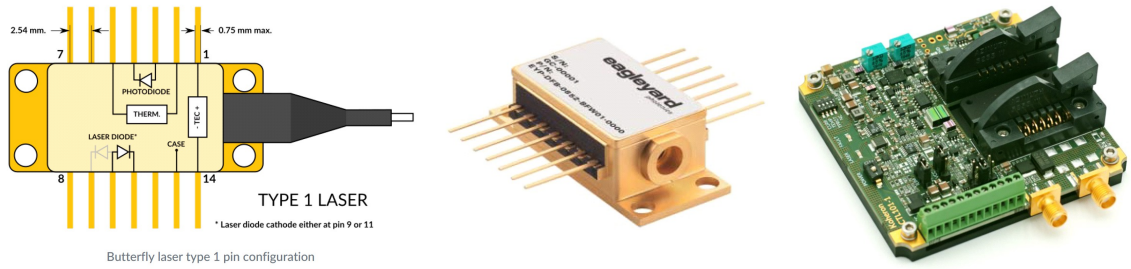

Figure 3.1: Left) shows a prototype of a butterfly type one laser. Middle) Toptica Eagleyard laser used in our setup. Right) Laser controller used in our setup. Taken from Ref.[1, 2, 3]

through both internal and external signals.

To stabilize the laser's operating frequency we use the following general approach. We first obtain an "absolute" atomic reference signal that corresponds to the targeted optical frequency. From this reference signal we derive an error signal that provides a voltage proportional to how far the actual frequency is from the target. Finally, the error signal is input to a controller that generates a feedback signal for the laser. Through feedback signal, the controller actively stabilizes the laser on the target frequency making it highly resilient against environmental effects. We now describe the rest of these steps in more detail.

3.1.1 The Reference Signal: Doppler-Free Spectroscopy

As discussed in chapter 2, we use Doppler-free rubidium spectroscopy to obtain reference signal corresponding to an absolute optical frequency at 780 nm. Here, we describe how this is realized in practice. Figure (3.2) shows the optical setup of the spectrometer.

To observe the rubidium spectrum, the laser current is scanned back and forth in frequency using a triangle wave generator with a period of 4 Hz. The amplitude of the scan determines the span of the frequency range, and the scan offset determines the laser's central operating frequency. To hone in on the targeted transition (the $F = 2 \rightarrow F' = 2(3)$ crossover in ^{87}Rb), we initially scan over a 1 GHz range to

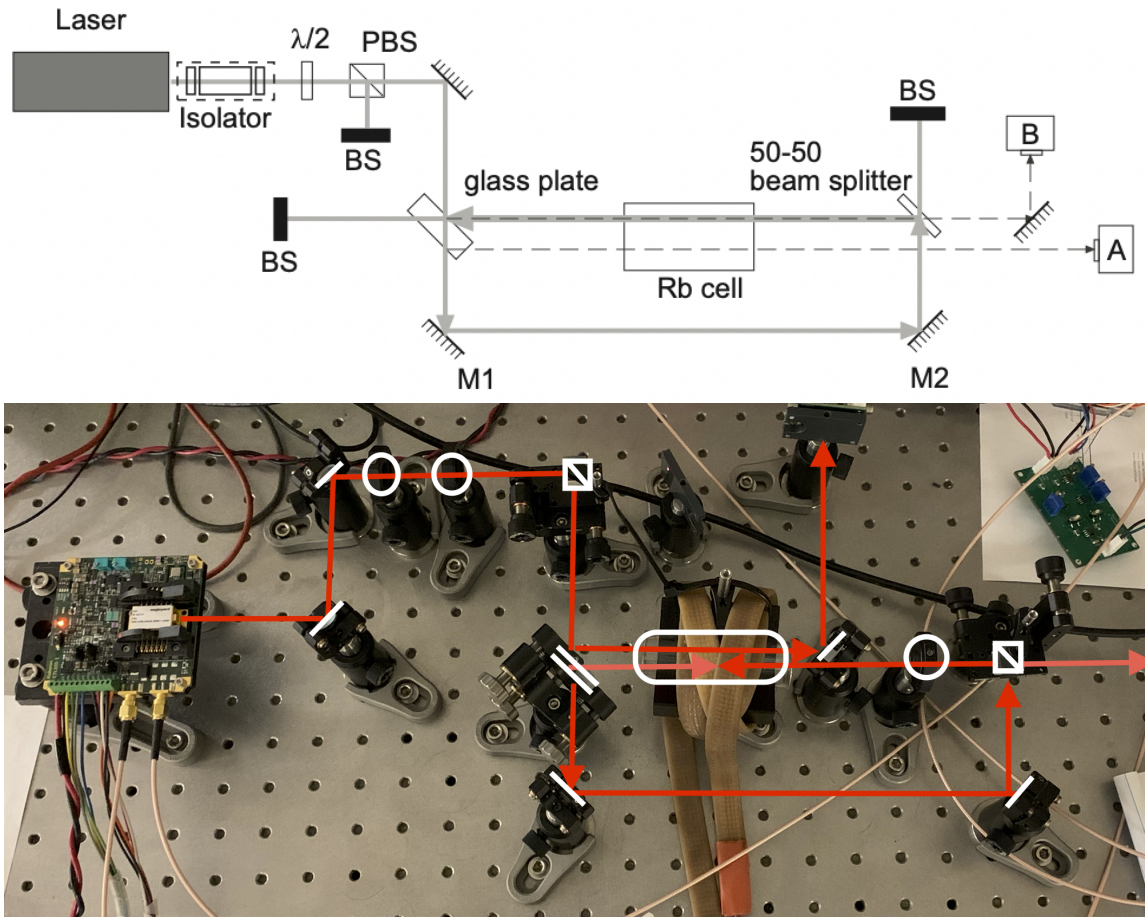

Figure 3.2: The experiment schematics (top) and setup (bottom) for Doppler-free spectroscopy [6]. Inclined line/M = mirror, Ovals/(λ/n) = waveplate, double line/thick rectangle = glass plate, square with a line = Polarized Beam Splitter (PBS), bright red/grey lines = pump beam and pale red/dashed lines = probe beam.

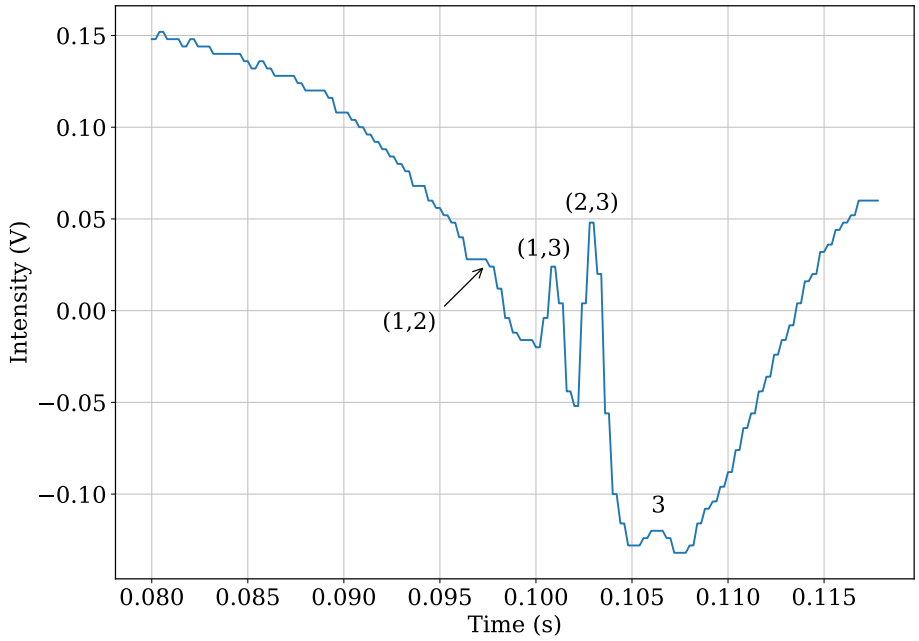

Figure 3.3: ^{87}Rb transition from F=2 to F'=3. The (1,2), (1,3) and (2,3) are the crossover peaks.

identify several saturated absorption peaks, and we gradually adjust the offset while reducing the amplitude until we are centred on the correct peak. This transition is an ideal reference for several reasons. First, it is the strongest absorption signal in ^{87}Rb, and is well separated from neighbouring peaks. This makes the laser lock more stable and robust against optical power and polarization changes. Second, it is near the cycling transition ($F = 2 \rightarrow F' = 3$) required for future laser cooling experiments.

3.1.2 The Error Signal: Modulating the Frequency of the Laser

Once the reference signal is obtained, the next step is to use it to derive an error signal. Generally, an error signal is the difference between the actual value and the desired set point of a system. In our case, the set point is the peak of the reference signal, which represents the atomic transition frequency, and the actual value is

the laser's operating frequency. The feedback controller will stabilize or "lock" the system to the point at which the error signal is zero. Because we wish to lock to the peak of the reference signal, ideally the error signal should be proportional to the first derivative of the absorption peak which feature a zero-crossing at the peak centre. Below we describe how we obtain this signal.

To obtain a signal proportional to the first derivative of the absorption peak, we use a frequency modulation scheme. Here, the laser's frequency is modulated with a small amplitude sine wave at frequency $f_{\text{mod}} = 100$ kHz while slowly scanning across the atomic resonance. This resulting absorption signal is then "demodulated" (i.e. it is mixed with the modulation signal and low-pass-filtered) using a lock-in amplifier to obtain the first derivative. To illustrate how this is achieved, we use the following mathematical model. The atomic absorption signal can be described as Lorentzian function,

$$A(f) = \frac{A_0}{1 + [2(f - f_0)/\alpha]^2}, \tag{3.1}$$

where A_0 is the amplitude of the signal, f_0 is the atomic resonance frequency, α is the full width at the half maximum (FWHM) or "linewidth" of the peak, and f is the laser frequency. The linear scan and sinusoidal modulation of the laser's frequency can be modeled by:

$$f(t) = at + b\sin(2\pi f_{\text{mod}} t), \tag{3.2}$$

where a and b are constants representing the scan rate and modulation amplitude, respectively. The modulated absorption signal is sent back to a lock-in amplifier, where it is multiplied by a sine wave of the same frequency as the modulation plus a controllable phase shift ϕ. The lock-in amplifier then averages the product of these two signals by passing it through a low-pass filter with a cut-off frequency below the modulation frequency. We model this filter by evaluating the time-average of this

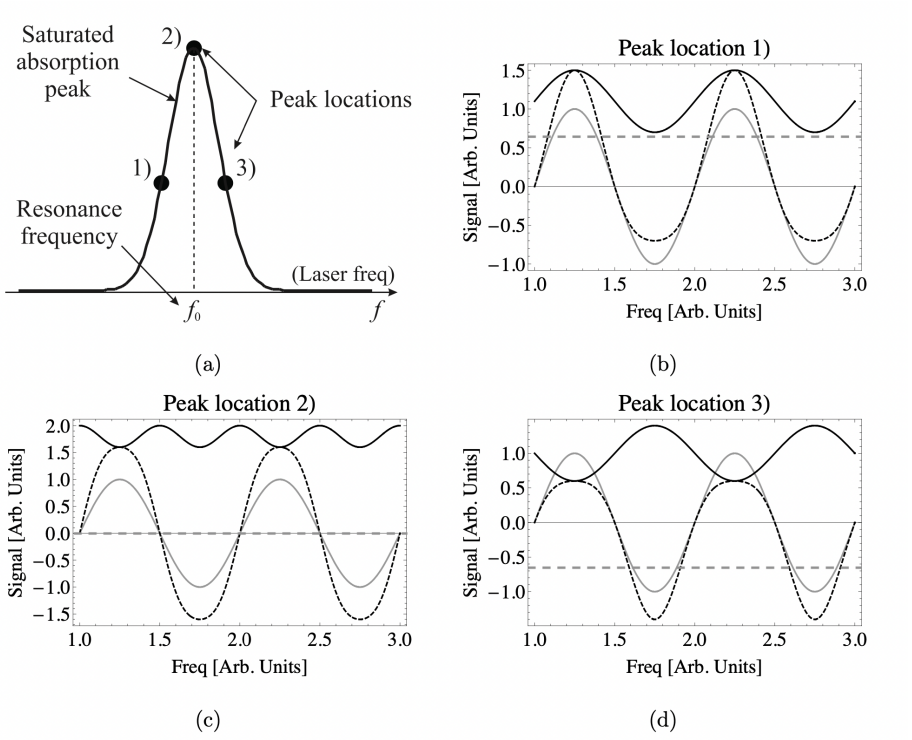

Figure 3.4: (a) Shows the saturated absorption around one of the peaks. Location 1) is the laser frequency before resonance, Location 2) frequency on resonance and location 3) after resonance. (b-d) Takes the photodiode signal (solid black line) multiplies it by the modulation signal (solid gray line) giving their product (dashed black line), where (the dashed gray line) is the sum of the product over the shown period of time. This shows the phase between the photodiode signal and the modulation changes between Location 1) and 3) and how that affects their product and its sum. Taken from Ref. [6]

product:

$$e(t) = \frac{1}{T}\int_t^{t+T} \frac{A_0}{1+[2(at' + b\sin(2\pi f_{\text{mod}}t') - f_0)/\alpha]^2} \sin(2\pi f_{\text{mod}}t' + \phi)dt', \qquad (3.3)$$

where $T = 1/f_{\text{mod}}$ is the period of the frequency modulation and ϕ is the phase shift introduced by the lock-in amplifier.

The modulation adds minor variations to the scan, so when the laser's frequency is close to resonance, the laser frequency will get closer and further from resonance with the same frequency as the modulation. This will increase and decrease the measured intensity by the photodiode at the same rate Fig.(3.4(b)&(d)). When

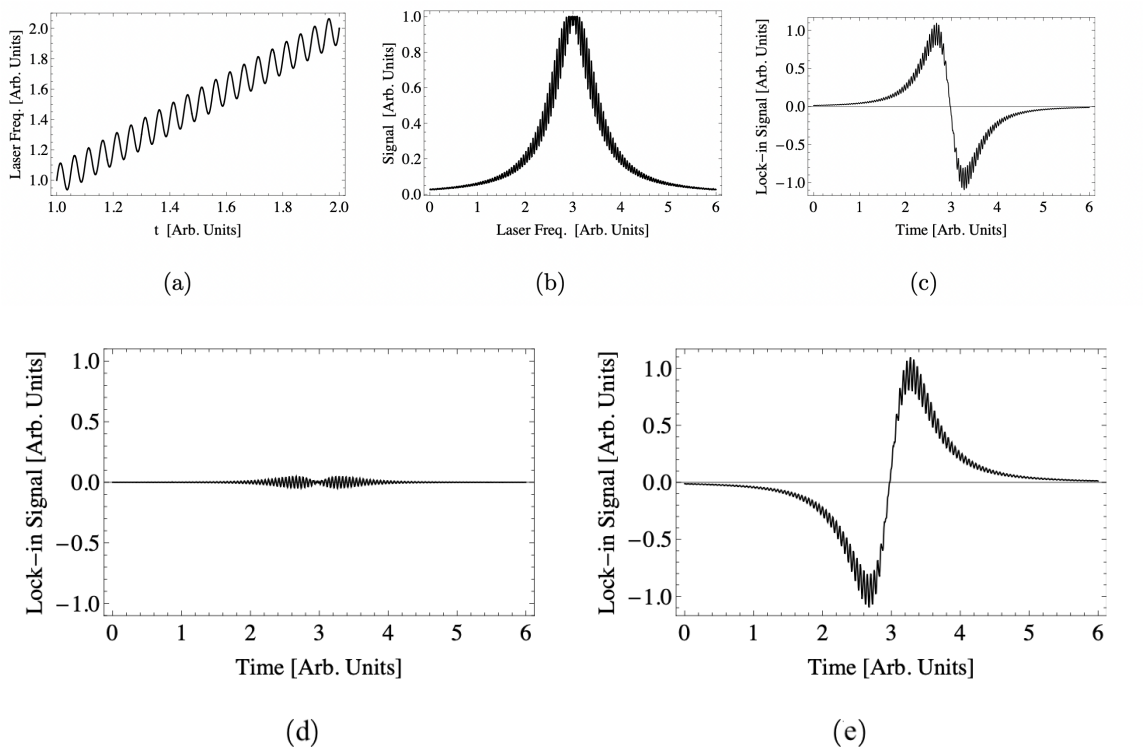

Figure 3.5: Graphical representation of: (a) The laser frequency, Eq.(3.2), (b) Lorentzian spectrum Eq.(3.1) and (c) The error signal Eq.(3.3), with ϕ the same as the phase shift of the photodiode signal. The error signal when the phase difference is (d) 90° (e) 180°. Taken from Ref. [6]

the laser is on resonance, the modulation will cause the laser to oscillate around the resonance Fig.(3.4(c)). The further the laser's frequency is from resonance, the smaller amplitude of the modulation affects the absorbed spectrum, compared to when the laser is closer to resonance Fig.(3.5(b)).

When the laser is before resonance, the product is mostly above zero, so the sum around that period will be positive. In contrast, the sum will be negative after resonance, and it will be zero on resonance. Near the resonance frequency, the error signal gives a measure of how far we are from resonance, which will be used by the PID controller to generate a feedback signal Fig(3.6).

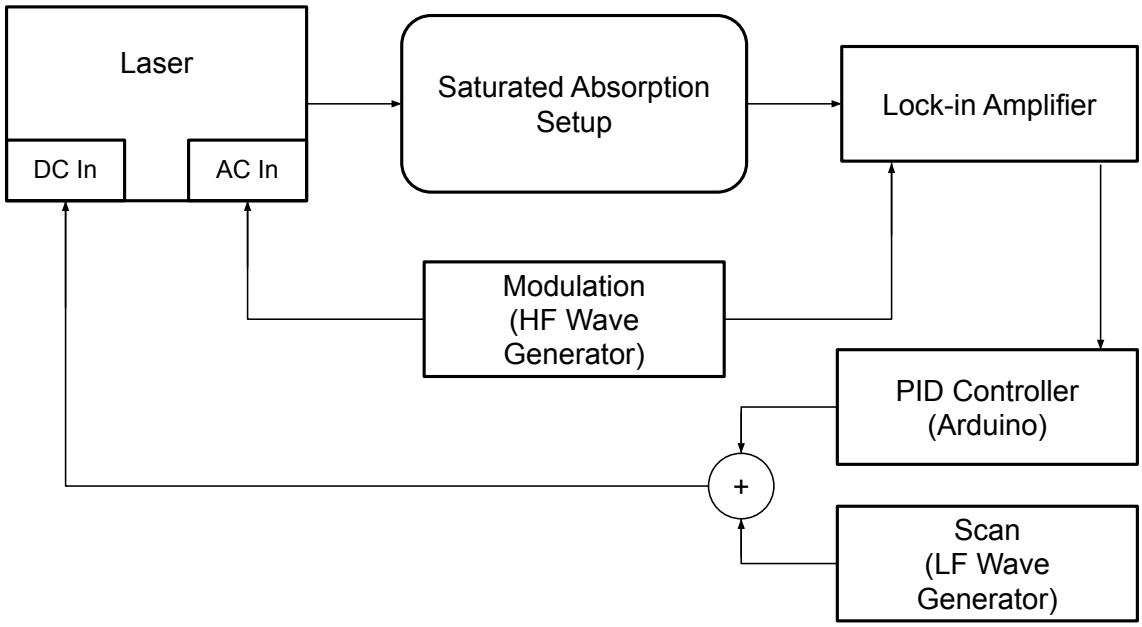

Figure 3.6: A block digram of the setup

3.1.3 The Feedback Signal: Making a PID Controller

The microcontroller in our setup is a PID controller [10], which uses the error signal $e(t)$ in its feedback loop to correct for the deviations from resonance. A PID controller makes corrections based on Proportional, Integrator, and Derivative terms. The proportional term takes the current error of the system and multiplies it by a proportional gain (K_p). The proportional term aims to decrease the error quickly, giving the controller a short reaction time. However, a pure proportional controller might not get the error to zero. For a system with a driving force that causes a higher error signal, K_p will cancel out its effect, but would not get the system in a state were the error signal is zero. An Integrator term can solve this problem by taking the sum of the error over time and multiplying it by the integrator gain K_I to eliminate any persisting error. High K_P or K_I can lead to oscillations, as they keep overshooting the zero error. The Derivative term takes the rate of change of the error and multiplies it by a derivative gain (K_D); this helps remove any oscillation in the output, by "predicting" the system's behaviour. The output of the PID controller

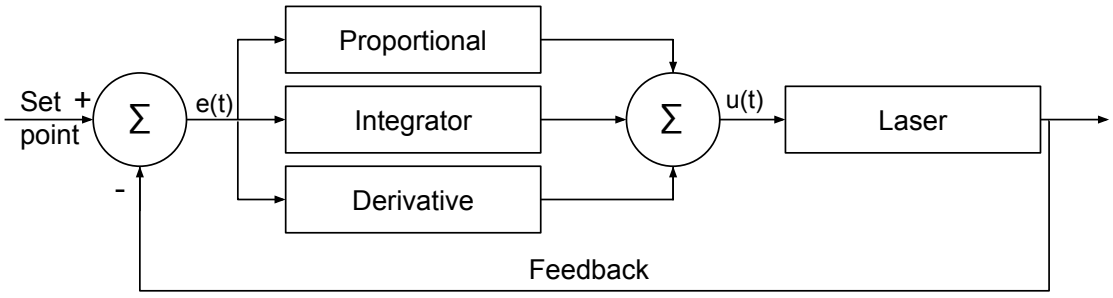

Figure 3.7: A block digram of the PID

$(u(t))$ is the sum of all of those terms,

$$u(t) = K_c \left(e(t) + \frac{1}{T_i} \int e(t)dt + T_d \frac{de(t)}{dt} \right) \tag{3.4}$$

where $K_c = K_P$, $K_I = \frac{K_c}{T_i}$ for the integral time T_i and $K_D = K_c T_d$ for the derivative time T_d.

3.2 Main Components Involved and their Role

In this section, we discuss experimental details relevant to the laser, our control electronics, and how we lock the laser in practice.

3.2.1 Laser

A Toptica Eagleyard (model: EYP-DFB-0780-00040-1500-BFW11-0005, type 1) laser is connected to a Koheron (model: CTL101-1-B-400) controller. The chip controls the current supplied to the laser and the laser's temperature [3]. The laser has a 780.24 nm centre wavelength and a linewidth of Full Width at Half Maximum (FWHM)$<$ 600 kHz with a maximum power of 40 mW [1]. The controller has a trimmer to adjust the temperature of the laser. There is another trimmer to offset the current supplied to the laser. The controller has two modulation inputs, a low frequency input (DC input) that accepts between DC and 10 MHz, with a range ± 1

volt, and a high frequency input (AC input) for modulation above 1 MHz with a gain of 20 mA/V. The DC input will accept the scan's and the Arduino's outputs Fig.(3.6). The scan's and the micro-controller outputs go through operational amplifiers to add their signals and rescale them to fit the DC input limits. The AC input will accept the modulation's output.

3.2.2 Lock in Amplifier

The lock-in amplifier serves two main purposes, the first is isolating the incoming signal and amplifying it; the second is generating an error signal. The lock-in amplifier uses the signal from the probe photodiode and a reference of the frequency of the modulation, to multiply the probe signal by a sine wave of the modulation frequency, this will generate the error signal as discussed in section(3.1.2). To isolate the probe signal from noise, a bandwidth of the signal is set on the lock-in amplifier. To get the highest error signal, the phase of the sine wave (ϕ, in Eq.(3.3)) created by the lock-in amplifier is changed to match the phase of the input photodiode. If the ϕ is shifted by 90 degrees, the error signal will be relatively close to zero Fig.(3.5(d)). While if the ϕ is shifted by 180 degrees, the error signal will be negative Fig.(3.5(e)). How the error signal behaves with the shift in ϕ helps find the right ϕ by setting the error signal to zero and then changing it by 90 degrees. The error signal is sent to the microcontroller.

3.2.3 Microcontroller

An Arduino Due is used as it is a relatively cheap option for a PID controller. The following table shows the advantages and the limitations of having a digital PID controller. The Arduino Due has six analog inputs (ADC) and two analog outputs (DAC) [9], each with a resolution of 12-bits (i.e., $2^{12} = 4096$ discrete input/output values). The sampling rate for the current setup is around 60 μs, making it well

Table 3.1: Advantages and disadvantages of digital PID control

Advantages	Disadvantages
Programmable: The system can be reprogrammed to implement different algorithms and methods.	Limited by its clock speed.
Reconfigurable: The system can be reconfigured to work with a different system.	Can not perform sequences in parallel.
Low cost: The digital components are relatively cheap as they are industrialized for different applications.	Limited by its ADC and DAC resolutions.
Compact: The overall size of the controller can be the size of a hand.	
Easy and Reliable: The system can be programmed using a high-level programming language, giving consistent outputs.	

suited to our application.

The analog inputs can only measure from ground up to 3.3 V. The lock-in amplifier output is set to be from -1 to 1 V Fig.(3.8 bottom). The error signal from the lock-in amplifier is passed through operational amplifiers Fig.(3.8 top) to change its amplitude to 1.65 V and offset the signal by 1.65 V, so the zero output from the lock-in amp corresponds to 1.65 V into the Arduino. This adjusts the scale such that 1 V (lock-in output) corresponds to 3.3 V (Arduino input) and -1 V (lock-in output) to 0 V (Arduino input). As the Arduino reads the input in bits, the readings get rescaled in volts, and the error signal is compared to the 1.65 V.

We decided not to use the derivative part in the PID in our cases (i.e. the derivative gain is set to zero.). The integrator part of the PID gets calculated by adding

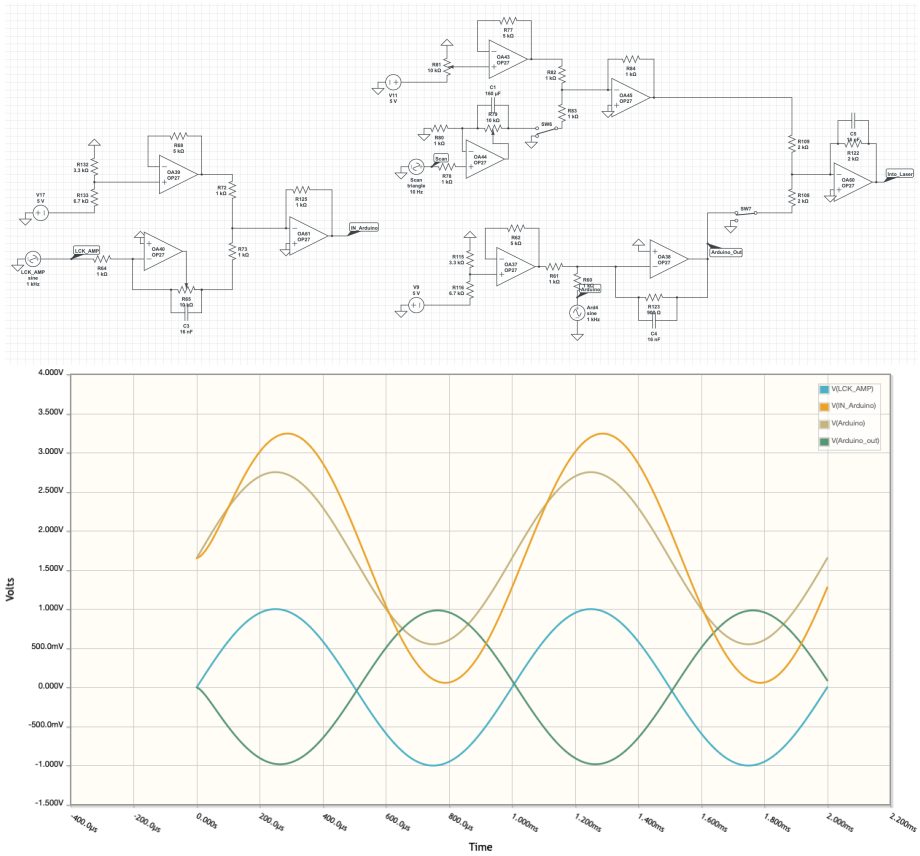

Figure 3.8: Top) A conditioning circuit that includes all the operational amplifiers used for rescaling voltages. Bottom) A graph showing how the voltage is rescaled from one of the setup components to another. Notice that the scan is not included as it will contribute only millivolts to the circuit, so it can be ignored. The circuit and the graphs were made using CircuitLab.com

the error over time. Anti-windup conditions (Algorithm(1)) are set to stop the controller from railing away if the error was significant or some disruption happened to the system, causing the error to increase drastically. The output signal (PID out) is the sum of the proportional and the integrator terms.

The Arduino's DAC receives data in bits, and it can only give output voltage from 0.55 V to 2.75 V. So, the output signal gets rescaled to bits. An offset of half the range of the bits is given to correspond to the zero error signal. Since the laser only accepts inputs from -1 V to 1 V, the output of the Arduino gets rescaled and offset by operational amplifiers, then gets added to the scan signal by another

Algorithm 1: An algorithm for the feedback signal from the Arduino

Let: Proportional Gain = Gp;
Let: Integrator Gain = Gi;
Let: AccumulatedError = AccErr;
Let: Integrator Upper Limit = iLimitUp;
Let: Integrator Lower Limit = iLimitDwn;
Let: Proportional Upper Limit = pLimitUp;
Let: Proportional Lower Limit = pLimitDwn;
$ReadInput \leftarrow analogRead(InputPin)$;
$Error \leftarrow (ReadInput/4095) * 3.3 - 1.65$;
$AccErr \leftarrow AccErr + Error * dt$;
if $Gi * AccErr \geq iLimitUp$ **then**
  $AccErr \leftarrow iLimitUp/Gi$;
end
if $Gi * AccErr \leq iLimitDwn$ **then**
  $AccErr \leftarrow iLimitDwn/Gi$;
end
/*The PID out is rescaled by dividing it by 2.2, then gets converted to bits and added an offset of half the range of the bits.*/
$OutputValue \leftarrow ((Gp * Error + Gi * AccErr)/2.2) * 4095 + 2048$;
/*Setting a limit to the Output value, not to overload the OutputPin*/
if $OutputValue \geq 4095$ **then**
  $OutputValue \leftarrow 4095$;
end
if $OutputValue \leq 0$ **then**
  $OutputValue \leftarrow 0$;
end
$analogWrite(OutputPin, OutputValue)$;

operational amplifier and sent to the laser.

3.3 Locking the Diode Laser

Finally to lock the laser on the reference resonance; the probe signal and the error signal are displayed on an oscilloscope, this helps with the transition peak visually Fig.(3.9(a)). Then the amplitude and the offset of the scan are adjusted to start zooming in on the chosen reference resonance. We keep zooming in until the error signal is almost linear Fig.(3.9(b)). Once we have a linear error signal displayed,

the Arduino is turned on and it locks the laser to resonance by minimizing the error signal to zero Fig.(3.9(c)). Finally the scan is turned off Fig.(3.9(d)), and the laser is locked to the desired reference resonance.

In the next chapter we discuss how different gains affect the PID reaction to the error signal, and the lock's short and long term stability.

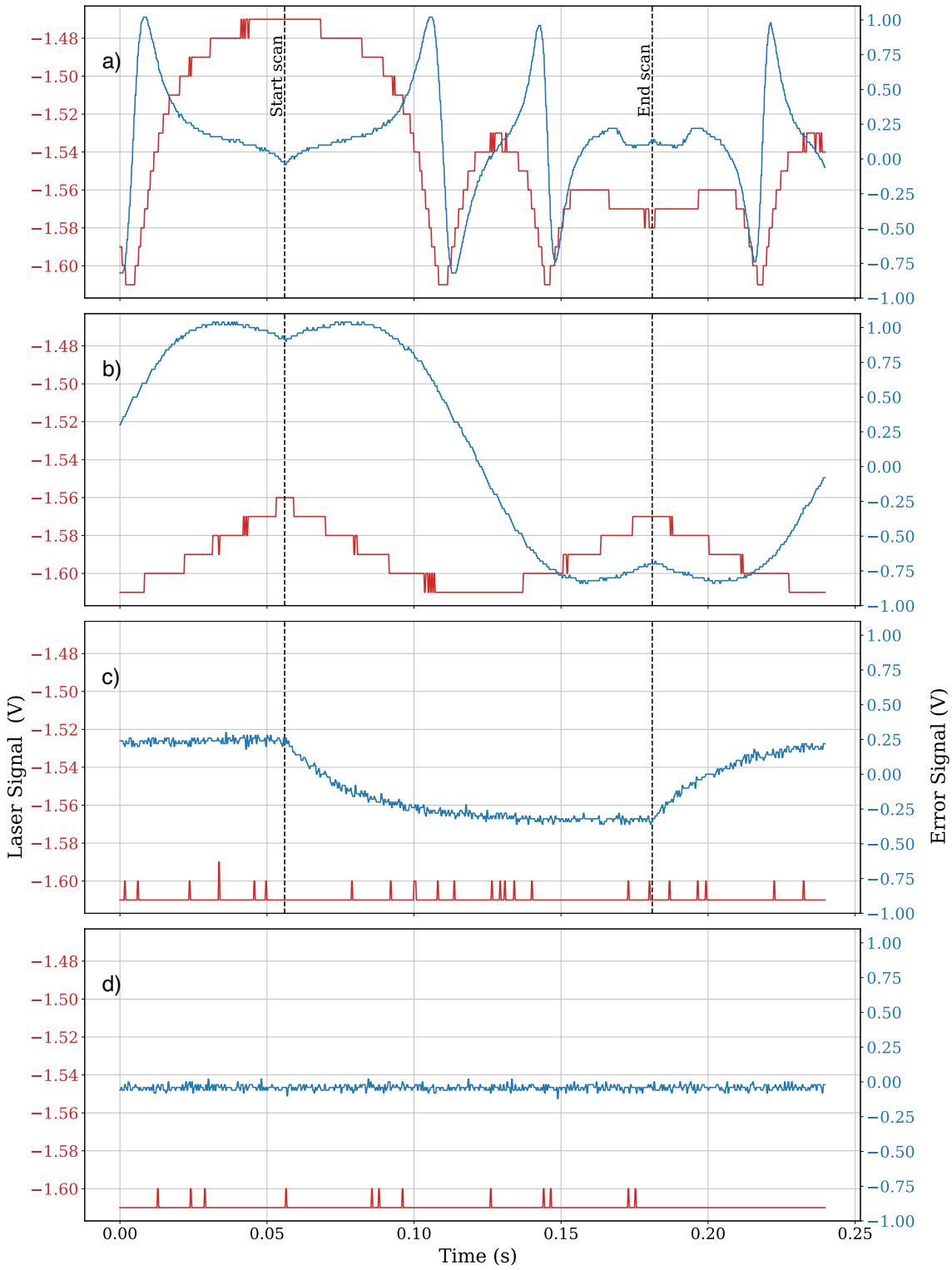

Figure 3.9: Plots showing the steps required to lock the laser to ^{87}Rb $F' = (2, 3)$. Any discontinuity signifies the start or the end of the scan's triangle wave. (a) Identify the transition peaks. (b) Zoom in until the error signal is almost linear. (c) Turn the PID on. (d) Turn the scan off.

Chapter 4

Characterization of the Laser Lock

The previous chapter presented our approach for locking the laser to a Doppler-free hyperfine transitions using a digital PI controller. In this chapter, we will further characterize the performance of the locking system in terms of several metrics. These include the response time of the lock, the optimal gains for the lock, and the short and long-term stability. First, we discuss our approach for calibrating the error signal. Then we present a technique to tune the gains of the PI controller. Finally, we describe how we analyzed the short- and long-term performance of the lock.

4.1 Calibration of the Error Signal

So far, the error signal is the only measurement we have to state how far the laser frequency is from resonance; however, the signal obtained is in volts, which in an arbitrary scale that depends on the system's parameters. In our case, the signal of interest is the laser's frequency deviation from resonance. To convert the error signal from voltage to relative optical frequency variation, we use a scan that includes two crossover transition peaks, as shown in Fig.(4.1). Here, the crossover $F' = (1, 3)$ in ^{87}Rb, and the crossover $F' = (2, 3)$ in ^{87}Rb are fitted to find the difference between the centres of the two peaks in terms of the time during the scan. These peaks are

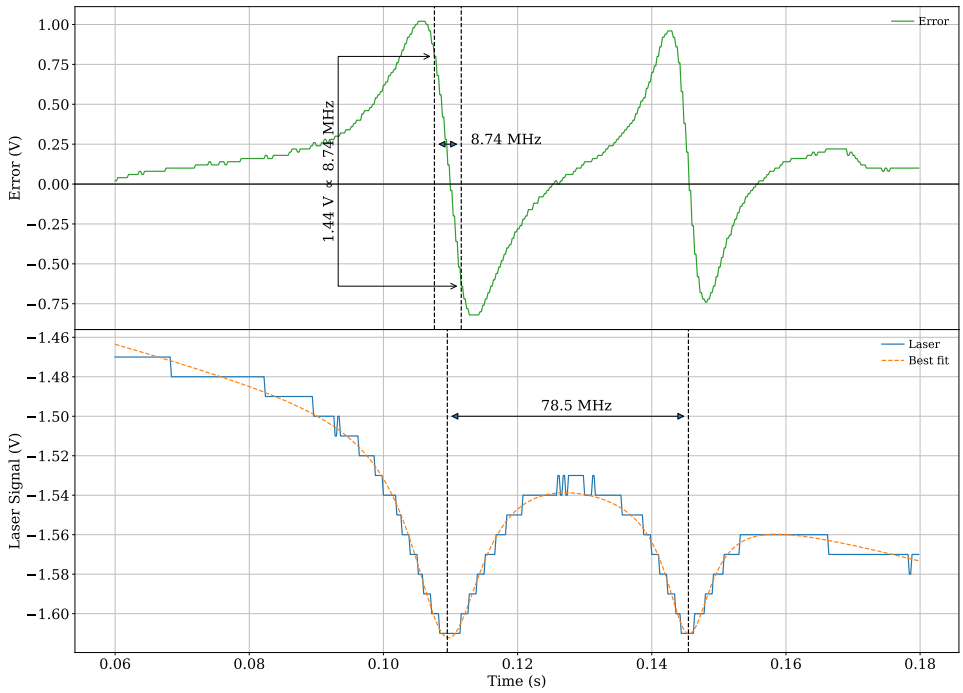

Figure 4.1: Plots to relate the variation in the error signal with the variation in the laser's frequency.

separated by precisely by 78.45 MHz, which allows us to relate the time interval in the scan to the change in the laser's frequency. From Fig.(4.1) we found that 78.5 MHz corresponds to $\approx$ 360 ms, so the conversion from time to laser frequency is 220 kHz/ms. This ratio is used to find the corresponding change in the laser's frequency over the linear part of the error signal. Finally from Fig.(4.1), the calibration factor for the error signal is $\approx$ 6.1 MHz/Volt. This relationship allows us to carry out the stability analysis in the next sections in physical units of the laser frequency.

4.2 Measuring the Impulse Response of the Lock

We characterized how the locking system behaves with different gain settings. Based on previous experience, my supervisor decided to set $K_d = 0$, as it can cause insta-

bilities to our system. One way to probe the lock is to measure its impulse response. This involves inducing a rapid impulse in the system and measuring how the error signal responds under different conditions. To achieve this, we send a square wave (impulse) signal to the laser current controller. The square wave aims to offset the laser's frequency in a rapid and constant manner to allow us to measure how the lock responds. In the presence of these impulses, we expect the lock to bring the error signal back to zero with different characteristics (e.g. decay rate, oscillation amplitude) depending on the values of the proportional and integrator gains, G_P and G_I. The proportional term, corrects for the error signal by multiplying it by G_p, giving an output in volts. The integrator term helps in correcting the error signal by taking its accumulation over time times the time step for each correction step times G_I. Let us call these gains with some arbitrary units K_P and K_I for the proportional and the integrator term respectively.

$$\begin{aligned}[K_P] &= \frac{\text{Volts of laser current modulation}}{\text{Volts of error signal}}, \\ [K_I] &= \frac{\text{Volts of laser current modulation}}{(\text{Volts of error signal})(\text{second})}.\end{aligned} \tag{4.1}$$

To express these gains in physical terms (i.e. optical frequency per V of error signal), we will need the calibration factor for the laser current frequency. From the documentation of the laser and the controller we are using, the calibration, S= (1.5 GHz/mA) x (2 mA/V) = 3000 MHz/V of the current modulation. The "physical gains" are then $G_P = SK_P$ and $G_I = SK_I$, and their units are now:

$$[G_P] = \frac{\text{MHz of laser frequency}}{\text{Volts of error signal}}, \qquad [G_I] = \frac{\text{MHz of laser frequency}}{(\text{Volts of error signal})(\text{second})}. \tag{4.2}$$

From eq.(3.4) we can rearrange for the integral time, $T_I = K_P/K_I$. Given K_P and K_I, T_I becomes the integral time constant τ_1, which describes the response time of the lock. High values of τ_1 means it takes longer for the lock to respond, while

smaller values of τ_1 means it takes shorter time to respond.

To model the impulse response of the error signal, we fit these data to an empirical expression that was developed based on a trial and error basis. The expression consists of an exponential term added to an exponential multiplied by a sine Eq.(4.3). The first term models the response time of the lock, while the second term models any decaying or growing oscillations, and describes the stability of the lock.

$$M(t) = A\left[\exp\left(\frac{-t}{\tau_1}\right) + \exp\left(\frac{-t}{\tau_2}\right)\sin\left(2\pi f t + \phi\right)\right] + c, \tag{4.3}$$

Here, A is the amplitude to model, τ_1 is the integral time constant, τ_2 is time constant for oscillations (a negative τ_2 describes growing oscillations while positive τ_2 describes decaying oscillations), f is the frequency of the oscillations, ϕ is the phase shift and c is an offset from zero. The offset could be a results of a small potential difference between the photodiode and the oscilloscope collecting the data. By extracting this parameters from data sets taken with different gain settings, we are able to quantify both the lock response time and stability. To quantify the stability of the lock we will use the following equation,

$$\mathcal{S} = \exp\frac{-3\tau_1}{\tau_2}. \tag{4.4}$$

Equation (4.4) aims to show how the response is acting after few τ_1s. Where, relatively high values of $\mathcal{S}$ shows instability and relatively low values, suggests stability. $\mathcal{S}$ and τ_1 will allow us to find the optimal settings for the lock.

4.3 Tuning the PI Controller

To tune the PI controller (i.e. to find the optimal gain settings), we surveyed the impulse response of the lock for a variety of gain settings. Specifically, eight sets of

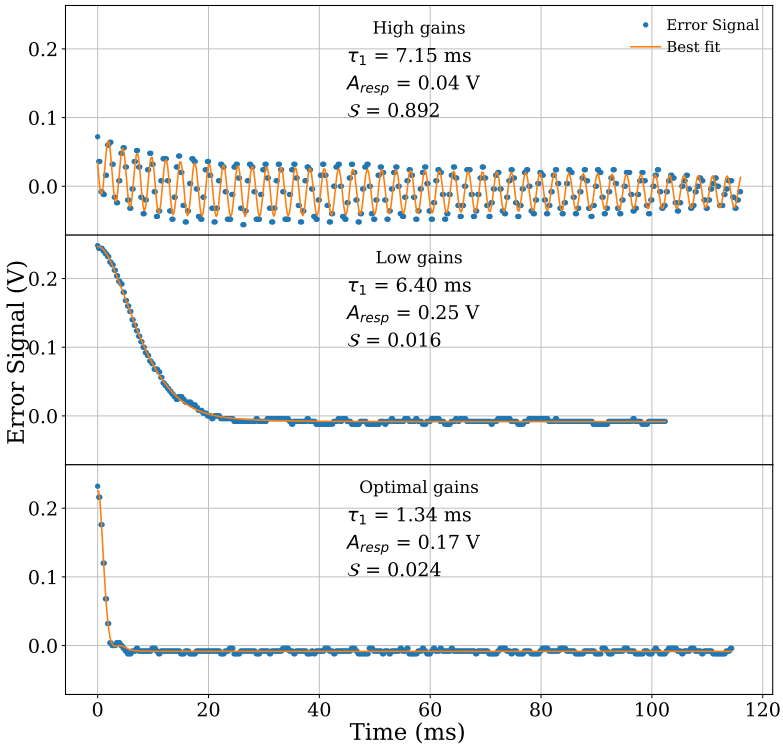

Figure 4.2: Plots to show the lock response with different gains. Top) Gets the fastest to the zero error but exhibits a lot of oscillations (K_P=7.0×10^{-2}, K_I=7.0×10^{-4}). Middle) Takes a long time to reach the zero error, exhibits no oscillations (K_P=1.0×10^{-3}, K_I= 5.0×10^{-5}). Bottom) Has the smallest τ_1 and exhibits no oscillations (K_P=7.0×10^{-3}, K_I=3.0×10^{-4}).

proportional gains (K_P= 7×10^{-2}, 5×10^{-2}, 3×10^{-2}, 1×10^{-2}, 7×10^{-3}, 5×10^{-3}, 3×10^{-3} and 1×10^{-3}) each with four integrator gains (K_i= 7×10^{-4}, 3×10^{-4}, 9×10^{-5} and 5×10^{-5}). The arbitrary gains can be converted to physical quantities by multiplying them with the calibration factor S. The gains were chosen based on previous experience aiming to show the limits of the lock and to find the optimal gains.

Figure (4.2) shows the how the system behaves with different sets of gains. Displaying τ_1, $A_{\text{resp}} = A$ and $\mathcal{S}$. As seen, high gains cause instability and take a relatively long time to lock; however due to the high gains A_{resp} is low. Low gains,

takes long time to lock, but is the most stable. The Optimum gains plot shows the fastest locking with high stability.

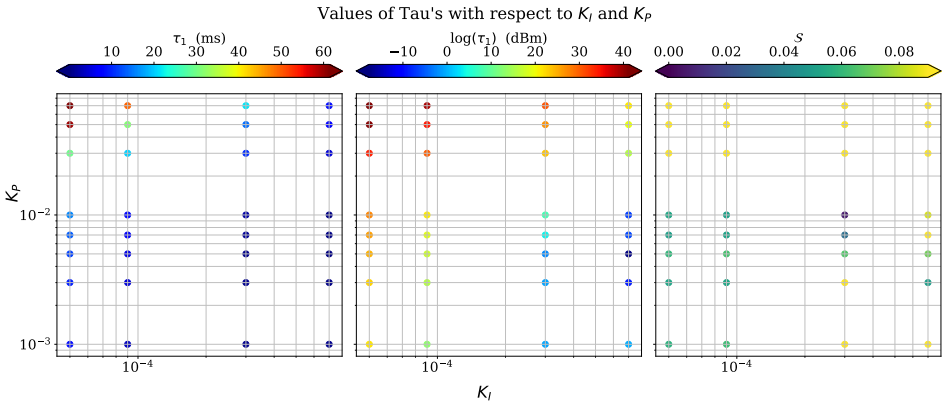

Figure 4.3: The response time and stability of the lock, with respect to K_P and K_I. The first two plots show the response time τ_1 in linear and logarithmic scales. The third plot shows the relative stability of the lock (lower values = more stable).

The surveyed data are fitted with eq.(4.3) to get τ_1 and $\mathcal{S}$. The first two plots of figure(4.3) display the values of τ_1, one with a linear scale and the other with logarithmic, the third plot identifies the stability of the lock. From the logarithmic plot, we find that for $K_I \leq 1 \times 10^{-4}$, the response time is the slowest. From $\mathcal{S}$'s plot we notice all the values of $K_P \geq 3 \times 10^{-2}$ are not stable. Finally, we found that the region of $K_I = 3 \times 10^{-4}$ and $5 \times 10^{-3} \leq K_P \leq 1 \times 10^{-2}$, gives the most stable and the fastest response time. From that region, the set of gains: $K_I = 3 \times 10^{-4}$ and $K_P = 7 \times 10^{-3}$, have the fastest response time of $\tau_1 = 1.34 \pm 0.05$ ms.

4.4 Short-Term and Long-Term Stability

In this section, we characterize the stability of the lock at both short and long timescales. For short timescales, we use the Power Spectral Density (PSD). By Fourier analyzing the error signal, the PSD allows us to display the changing of the relative optical frequency for each component of the frequencies of the Fourier

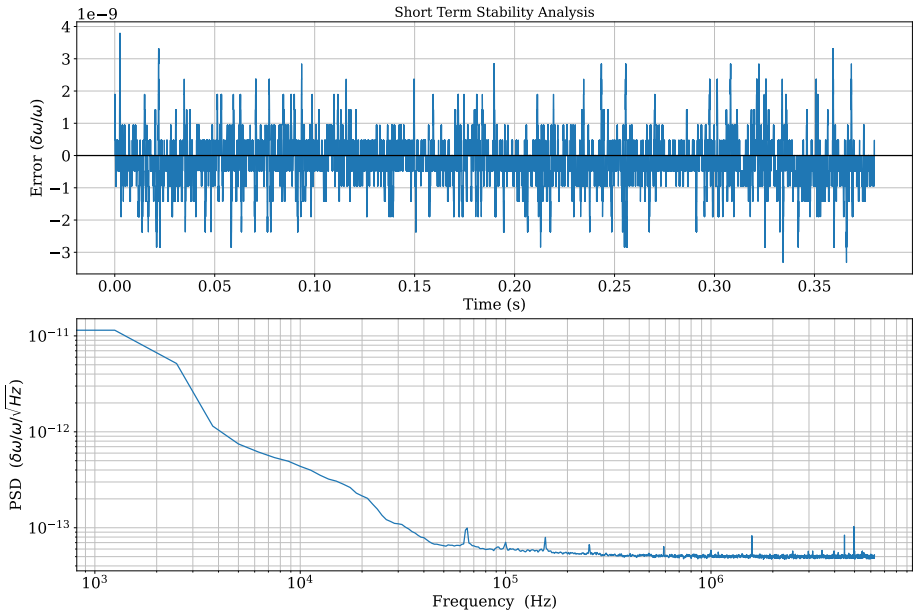

Figure 4.4: (a) High-resolution measurement of the laser frequency variation over 380 milliseconds. (b) The Power Spectral Density (PSD) graph of the error signal to identify noise. The white noise floor has a PSD value of $5 \times 10^{-14}/\sqrt{\text{Hz}}$.

transform. This will help us to identify different types of noise (pink noise, white noise, ...) and the contributors to the change in the laser's frequency.

For longer timescales, we use the Allan deviation, as it is the standard for measuring frequency stability. The Allan deviation calculates the square root of the Allan variance (a measure of frequency stability) for a specific time step. As for longer time periods any white noise should average to zero, so, for bigger time steps the Allan deviation keeps getting smaller in value [21].

Figure(4.4) shows what we call a high resolution dataset (4 million and 750 thousands points with a time step of 80 ns) of the changes in relative optical frequency of the laser as it is locked with the scan off. From the PSD part of the graph, starting from $\sim$ 1.2 kHz to 40 kHz the PSD shows a $1/f$ relationship which indicates pink noise. The pink noise is due small fluctuations in the configuration of any defected materials and fluctuations in the properties of semi-conductors [20]. From $\sim$ 200 kHz until the end of the graph, is white noise (ignoring the individual peaks), which is mainly unavoidable electric noise, and it resembles our limit for minimizing the

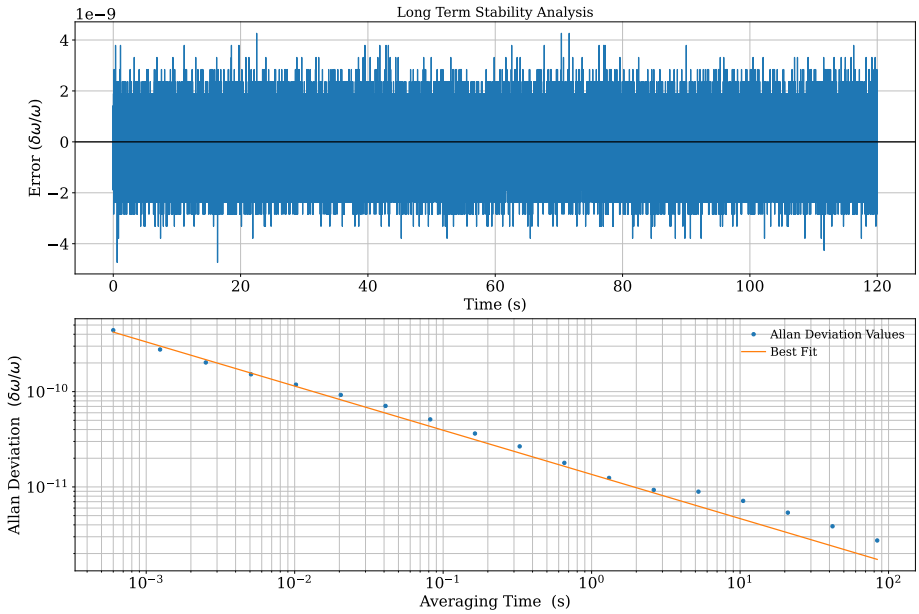

Figure 4.5: (a) High-resolution measurement of the laser frequency variation over 120 seconds. (b) The Allan deviation graph of the variation of the frequency variation to identify the stability of the lock. The Allan deviation of the fractional frequency variation of the short-term stability (at 1 second) is $(1.35 \pm 0.14) \times 10^{-11}$ and the medium term stability (at 84 seconds) is $(2.74 \pm 14) \times 10^{-12}$.

noise, at PSD value of $5 \times 10^{-14}/\sqrt{\text{Hz}}$. The effects of the noise are ignorable as they barely contribute to the change of the laser's frequency. The peaks that appear after 1 MHz are noise from the current control of the laser's controller [3]. To show the contribution of the white noise to the variation of the laser's frequency, over a period of 1 MHz (from 2 MHz to 3 MHz), the change in the PSD is around 1×10^{-14} (from 4×10^{-14} to 5×10^{-14}). The relative change in the laser's frequency $\sigma_{\Delta f}$ equals the change in the PSD $S_{\Delta f}$ times the square root of the change in frequency Δf. So, $\sigma_{\Delta f} = 1 \times 10^{-14} \cdot \sqrt{1 \times 10^{6}} = 1 \times 10^{-11}$. The laser's frequency is around 384.230 THz, so the change in laser's frequency $= 1 \times 10^{-11} \cdot 3.8423 \times 10^{14} = 3.8423$ kHz which is much smaller than the laser's lindewidth (600 kHz)[1]. This shows that the laser is highly stable on the short-term.

For the long-term stability, figure(4.5) shows another high-resolution dataset (6 million data points with a time step of 40 μs) of the laser's frequency variation over

120 seconds. As we expect the plot to keep decreasing over time, we fitted using a power law to find it is decreasing with the square root of time. From the fit we were able to obtain the the value of the Allan deviations for a small time step, 1 second to be $(1.35 \pm 0.14) \times 10^{-11}$, while at a medium time step like 84 seconds, we found the deviation to be $(2.74 \pm 14) \times 10^{-12}$ which is considered to quite stable. To find the true stability of the lock, the error signal needs to be measured over long enough period of time, that the Allan deviation reaches a bottom limit, then it starts to increase. As our dataset is not long enough, we can not determine the true stability of our lock.

Chapter 5

Conclusion and Future Work

5.1 Conclusion

The main goal of this thesis project is to stabilize a laser to an atomic reference using a microcontroller. To achieve this goal, we reviewed several key elements related to this study. First, we presented the principles of optical spectroscopy and how to obtain narrow spectral features that are free from Doppler broadening due to the temperature of the atoms. We discussed rubidium gas and its electronic structure, as this serves as an absolute atomic reference for locking our laser. Using our vapour cell rubidium sample, we measured the hyperfine transitions on the D_2-line at 780 nm using Doppler-free spectroscopy. We identified several absorptions peaks in ^{85}Rb and ^{87}Rb, and used the strongest crossover peaks to calibrate the frequency scan of the laser.

We then showed how, by combining a lock-in amplifier and a frequency-modulated absorption spectrum, we can generate an error signal that is proportional to the laser's deviation from the target frequency. The error signal features a zero-crossing at the peak of the absorption signal, which is mostly insensitive to environmental factors. This crucial part of the experiment allows us to precisely lock the laser

frequency using a PID controller, which enables us to realize a stable optical reference at 780.24 nm.

The PID controller is implemented using a commercial microcontroller (an Arduino DUE) with built-in 12-bit ADCs and DACs. We designed and built an analog conditioning circuit to rescale the voltage range of the input and output signals used with the microcontroller. This circuit was implemented on a printed circuit board and assembled in a shielded chassis to reduce ambient electronic noise.

Following an initial demonstration of the lock, we characterized the performance of the lock in several ways. First, we tuned the PID controller to find the optimum values for the proportional and integrator gains (we set derivative gain to zero). Then we measured the PSD and the Allan deviation of the error signal to determine the noise characteristics and the short- and long-term stability of the locked laser. From the PSD, we found that the noise is limited by pink noise (i.e. $1/f$ noise) at frequencies in the range of 1 - 100 kHz. Above these frequencies, the error signal is dominated by white noise. In terms of the fractional frequency variation of the laser, we measured a noise floor of $5 \times 10^{-14}/\sqrt{\text{Hz}}$.

The Allan deviation of the error signal shows a $1/\sqrt{\tau}$ dependence for our measured timescales (up to 120 s), which is consistent with white noise. From this Allan deviation, we find a short-term fractional frequency stability of 1.3×10^{-11} at 1 s, and a medium-term stability of 2.7×10^{-12} around 90 s. Both of these values indicate that the laser is extremely stable over medium periods. Longer data sets are required to determine the limiting behaviour of the lock.

5.2 Future Work

As for the current stage, more data will be gathered to have a better characterization of the lock; testing more gain sets and analyzing the lock's stability over long periods

to find its absolute stability.

This work has highlighted how simple and intuitive it is to implement control algorithms with an Arduino. For future stages, we are already considering how this powerful tool can be used for a variety of other applications in our laboratory. With respect to the laser lock, we are planning several improvements. First, the PID program will be optimized more, to ensure faster handling of incoming data, increasing its bandwidth/decrease its loop time. Then, with a more optimized program we will be able to implement more sophisticated logic, increasing the flexibility and robustness of the lock to external changes. If the bandwidth of the improved system allows, the Arduino will generate the error signal replacing the lock-in amplifier. Second, we will investigate more robust (and less time consuming) methods for determining the optimum combination of gains for the PID controller. One such method would include solving for the gains analytically. Finally, we will try alternate methods for generating the error signal (e.g. polarization spectroscopy [19]) that do not require frequency modulation or a lock-in amplifier.

Bibliography

[1] EYP-DFB-0780-00040-1500-BFW11-0005, Rev. 0.91.

[2] Koheron CTL101 User Guide. https://www.koheron.com/support/user-guides/ctl101/, Accessed March 2022.

[3] koheron CTL101 Laser Guide. https://www.koheron.com/photonics/ctl101-laser-controller, Accessed March 2022.

[4] "Rubidium 85 D Line Data" by Daniel Adam Steck, 2009 University of Oregon - http://steck.us/alkalidata/

[5] "Rubidium 87 D Line Data" by Daniel Adam Steck, 2009 University of Oregon - http://steck.us/alkalidata/

[6] "Lab 4 – Laser Frequency Stability and the Lock-In Amplifier", in PHYS4061 Laboratory Manual, edited by B. Barrett, A. Carew, A. Kumarakrishnan, York University, Toronto (2013).

[7] "Lab1-EOM-Writeup-2013", in PHYS4061 Laboratory Manual, edited by B. Barrett, A. Carew, A. Kumarakrishnan, York University, Toronto (2013).

[8] "Lab2-Zeeman-Writeup-2013", in PHYS4061 Laboratory Manual, edited by B. Barrett, A. Carew, A. Kumarakrishnan, York University, Toronto (2013).

[9] Arduino Store "Arduino Due". https://store.arduino.cc/products/arduino-due, Accessed March 2022.

[10] R. P. Borase et al., "A review of PID control, tuning methods and applications", Int. J. Dynam. Control **9**, 818–827 (2021). https://doi.org/10.1007/s40435-020-00665-4

[11] Lumen Learning "Formation of Spectral Lines" https://courses.lumenlearning.com/astronomy/chapter/formation-of-spectral-lines/, Licensed Astronomy provided by OpenStax CNX, accessed March 2022.

[12] C. S. Adams, M. Sigel and J. Mlynek, "Atom optics", Phys. Rep. **240**, 143-210 (1994).

[13] S. Beattie et al, "First accuracy evaluation of the NRC-FCs2 primary frequency standard", Metrologia **57**, 035010 (2020).

[14] A. D. Cronin, J. Schmiedmayer, and D. E. Pritchard, "Optics and interferometry with atoms and molecules", Rev. Mod. Phys. **81**, 1051 (2009).

[15] "Handbook of atomic, molecular, and optical physics", Edited by G. W. Drake, Springer (1996).

[16] S. Haroche, "Essay: Fifty Years of Atomic, Molecular and Optical Physics in Physical Review Letters", Phys. Rev. Lett. 101, 160001 (2008).

[17] D. R. Leibrandt and J. Heidecker, "An open source digital servo for atomic, molecular, and optical physics experiments", Rev. Sci. Instrum. **86**, 123115 (2015).

[18] C. E. Wieman and L. Hollberg, "Using diode lasers for atomic physics", Rev. Sci. Instrum. **62**, 1 (1991).

[19] M. L. Harris et al, "Polarization spectroscopy in rubidium and cesium", Phys. Rev. A **73**, 062509 (2006).

[20] Kogan, Shulim, “Electronic Noise and Fluctuations in Solids”, Cambridge University Press,(1996).

[21] Cutler, L. S.; Searle, C. L., “ Some Aspects of the Theory and Measurements of Frequency Fluctuations in Frequency Standards”, Proceedings of the IEEE (1966)